Comparison of carbon in shungite rocks to other natural carbons: An X-ray and TEM study

V.V. Kovalevski[a],[*], Peter R. Buseck[b], J.M. Cowley[c]

[a]*Institute of Geology, Karelian Research Center, Russian Academy of Sciences, Pushkinskaya St. 11, Petrozavodsk 185610, Russia*
[b]*Departments of Geology and Chemistry/Biochemistry, Arizona State University, Tempe, AZ 85287-1404, USA*
[c]*Department of Physics and Astronomy, Arizona State University, Tempe, AZ 85287-1504, USA*

Abstract

The shungites of Karelia (Russia) form a large, diverse group of black Precambrian rocks, all of which contain an intriguing type of poorly crystalline carbon. Wide differences of opinion exist about its structural state and its relation to carbon from other geological environments and origins. We used a variety of measurement techniques to determine the structural features of the carbon in shungite samples and to relate them to other natural sources of carbon. Although there is a wide range of types of shungite rocks, it appears as if the structure of their carbon is similar throughout in respect to high-resolution transmission electron microscopy (HRTEM) images, and electron and X-ray diffraction patterns. Other samples whose carbon is indistinguishable using these techniques include those from the Erickson gold mine (Canada), the Sovetskaya gold mine (Russia), and the Sudbury impact structure (Ontario). Carbon samples from different localities of the Shunga district are characterized by containing curved layers, similar to samples from natural and synthetic cokes. The HRTEM images and nanodiffraction patterns of shungites suggest that some 3-dimensional closed shells occur but, more commonly, there are fractions of such shells or regions of structure that are highly disordered into bent stacks of graphene layers. © 2001 Elsevier Science Ltd. All rights reserved.

Keywords: A. Amorphous carbon; C. Transmission electron microscopy (TEM), X-ray diffraction; D. Microstructure

1. Introduction

Elemental carbon is widespread in the geological environment. In high-temperature rocks it occurs in well-crystallized forms, most commonly as graphite but also as diamond. Where it occurs in low-temperature rocks, generally as the result of organic decay, it typically is noncrystalline or poorly crystalline. Such carbon has been the focus of extensive studies (e.g. [1–9]) as have been the changes that occur during its progressive structural ordering [10].

One of the more intriguing types of poorly crystalline carbon occurs in the shungite rocks of Karelia (Russia). Shungites form a large, diverse group of black Precambrian rocks, all of which contain free carbon. They occur over thousands of square kilometers in Karelia and are a major geologic feature in that part of the world and perhaps elsewhere [11]. The first natural occurrence of fullerenes was reported from Shunga rocks [12].

Both the abundance and seemingly unusual physical characteristics of the carbon in shungites has made it a subject of attention as well as controversy. Inostrantsev [13], using the term to refer to the carbon and comparing it to coal, stated that shungite is an extreme example of noncrystalline carbon rather than a coal. On the other hand, according to Timofeyev [14] shungite is a bituminous coal similar to anthraxolite. Rankama [15] considered the possibility that the most carbon-rich shungite («type-I»; see Buseck et al., [11] for definitions of types) may be a carbonized hydrocarbon. Volkova and Bogdanova [16] believe that shungite is Precambrian coal with a wood-like morphology. According to Buseck and Huang [6] and Buseck et al. [17], the structural organization of carbon from types-I and -V shungites is comparable to kerogen of Precambrian age in the chlorite zone. Some petroleum geologists and others believe that shungite is a highly

Table 1
Summary of d-spacings, peak widths and apparent coherent lengths, L_c and L_a of the samples, listed in order of SAED and HRTEM degree of ordering. Column #2 indicates figure numbers with HRTEM images and XRD patterns resembling those of the respective samples[a]

Sample, locality	Fig.	HRTEM	SAED		XRD					
		d_f (nm)	L_c (nm)	L_a (nm)	d_1 (nm)	FWHM$_1$ (2θ) (CuK$_\alpha$)	L_c (nm)	d_3 (nm)	FWHM$_3$ (2θ) (CuK$_\alpha$)	L_a (nm)
Group 1										
Bitumen, Los Angeles, CA	1,6a	0.36–0.5	–	–	0.52	20	0.4	–	–	–
Group 2										
Asphaltum, Santa Barbara Co., CA	2,6a	0.35–0.5	–	1.4	–	–	–	–	–	–
Albertite, New Brunswick, Canada	2,6b	0.34–0.5	–	1.6	0.48 & 0.347	9 & 2.9	0.9 & 2.8	–	–	–
Pyrobitumen, Hatyspyt fm., Siberia	2,6a	0.35–0.47	–	1.7	0.47	12	0.7	–	–	–
Pyrobitumen, Elliot Lake, Ontario	3,6a	0.35–0.5	–	1.6	–	–	–	–	–	–
Group 3										
Asphaltite, Standard mine, CA	3,6b	0.36–0.43	1.8	1.6	–	–	–	–	–	–
Impsonite, Maine	3,6b	0.35–0.45	1.9	1.7	0.43 & 0.35	10 & 3.1	0.8 & 2.6	–	–	–
Cannel coal, Wigan, UK	3,6b	0.34–0.42	2.0	1.8	0.47 & 0.352	12 & 5.1	0.7 & 1.6	–	–	–
Pyrobitumen, Gunflint fm., Canada	3,6c	0.34–0.36	2.1	1.8	0.342	3.4	2.4	0.121	20	1.1
Pyrobitumen, Gunflint fm., Ontario	3,6c	0.33–0.35	2.1	2.1	0.344	3.0	2.7	0.122	10	2.1
Pyrobitumen, Gunflint fm., Ontario	3,6c	0.34–0.38	1.8	2.0	–	–	–	–	–	–
Group 4										
Adamsite, Atoka, Oklahoma	4,6b	0.34–0.44	3.0	1.6	0.48 & 0.35	10 & 2.6	0.8 & 3.1	–	–	–
Anthracite, Iserl, La Motte, France	4,6d	0.34–0.42	1.6	2.1	0.348	6.0	1.4	0.121	8.0	2.6
Anthracite, Canada	4,6d	0.34–0.4	1.8	1.6	0.348	5.0	1.6	0.119	15	1.4
Anthracite, Aveiro, Portugal	4,6d	0.34–0.41	1.6	2.8	0.351	7.0	1.2	0.121	8.0	2.6
Anthracite, Primrose Seam, PA	4,6d	0.33–0.42	1.2	2.5	–	–	–	–	–	–
Anthracite, Chrustaljnaja, Woodjanaja Ravine, Russia	4,6d	0.35–0.42	1.2	1.9	0.348	5.8	1.4	0.122	9.0	2.3
Pyrobitumen, Mesabi, Minnesota	4,6d	0.35–0.39	2.5	2.1	0.348	5.5	1.5	0.122	7	3.0
Meta-anthracite, Michigamme shale, Michigan	4,6e	0.34–0.37	1.9	3.7	0.348	4.4	1.9	0.121	5.5	3.8
Carbonaceous matter, Bakyrchik gold deposit, Kazakhstan	4,6e	0.34–0.4	1.4	3.4	0.351	6.2	1.3	0.121	5.8	3.6

Group 5

Carbon from type-I shungite rock, Chebolaksha	5,6e	0.34–0.36	1.8	3.7	0.347	4.4	1.9	0.1223	4.7	4.5
Carbon from type-III shungite rock, Chebolaksha	5,6e	0.34–0.37	1.9	4.0	–	–	–	–	–	–
Carbon from type-I shungite rock, Maksovo	5,6e	0.34–0.36	1.8	4.0	0.349	5.0	1.6	0.121	5.0	4.2
Carbon from type-I shungite rock #1, Maksovo	5,6e	0.34–0.38	1.9	4.3	0.346	4.2	1.9	0.1223	6.0	3.5
Carbon from type-I shungite rock #2, Maksovo	5,6e	0.34–0.36	1.9	4.0	0.349	4.6	1.8	0.122	5.0	4.2
Carbon from type-I shungite rock #3, Maksovo	5,6e	0.34–0.38	1.6	3.1	–	–	–	–	–	–
Carbon from type-I shungite rock #4, Maksovo	5,6e	0.34–0.39	1.7	3.1	–	–	–	–	–	–
Carbon from type-I shungite rock, Nigozero	5,6e	0.35–0.38	1.7	3.3	0.352	6.4	1.3	0.122	4.5	4.7
Carbon from type-I shungite rock, Shunga	5,6e	0.34–0.37	1.9	4.0	0.347	4.5	1.8	0.122	4.5	4.7
Carbon from type-II shungite rock, Shunga	5,6e	0.34–0.37	1.8	3.3	–	–	–	–	–	–
Carbon from type-I shungite rock, Sujsari	5,6e	0.35–0.38	2.0	3.3	0.350	5.8	1.4	0.122	4.8	4.4
Carbon from type-I shungite rock, Zazhogino	5,6e	0.34–0.36	1.8	4.0	0.347	4.4	1.9	0.1223	3.9	5.4
Carbon from type-III shungite rock, Zazhogino	5,6e	0.34–0.38	1.7	3.1	–	–	–	–	–	–
Natural coke, Jewett Brothers Mine, Chesterfield Co., VA	5,6c	0.33–0.38	1.9	4.7	0.345	2.5	3.3	0.122	20	1.0
Carbonaceous matter, Erickson gold mine, Canada	5,6e	0.34–0.38	1.8	3.3	0.350	5.4	1.5	0.122	4.6	4.6
Carbonaceous matter, Sovetskaya gold mine, Yenisej, Siberia	5,6e	0.34–0.37	2.3	4.3	0.348	5.2	1.6	0.122	4.8	4.4
Pyrobitumen, Sudbury, Ontario	5,6e	0.34–0.37	2.1	3.7	0.345	4.2	1.9	0.122	5.4	3.9
Pyrobitumen, Sudbury, Ontario	5,6e	0.34–0.36	1.7	2.9	0.346	4.4	1.9	0.121	4.5	4.7

[a] d_f–distance between adjacent fringes; d_1–diffraction maximum (maxima) near the *002* graphite peak; d_3–diffraction maximum near the *110* graphite peak; Blanks indicate the SAED or X-ray parameters could not be determined because of peak breadths or interferences from impurities.

evolved bitumen [18–23], and Khavari-Khorasani and Murchison [24] interpreted it as a pyrobitumen. According to Melezhic et al. [25], carbon from type-I shungites resulted from migrated bitumen, and carbon from type-III shungites is a mixture of kerogen residues and migrated bitumen.

The structure of the carbon in shungite rocks has been studied since 1937. Boldyrev and Kovalev [26] concluded from powder X-ray diffraction (XRD) studies that type-I shungite consists of dispersed graphite. Kviecinska [27] used XRD and electron diffraction to conclude that this carbon is similar to Ceylon graphite. Grew [3], using XRD, determined that type-I shungite is poorly ordered, and Usenbaev et al. [28] found by XRD that shungite contains graphitic layers, but that even at 2800°C it does not transform to graphite. From optical and XRD studies, Khavari-Khrasani and Murchison [24] determined the presence of aromatic layers that form stacks and that the carbon in the Karelian shungite samples they examined did not correspond to graphite. By using high-resolution transmission electron microscopy (HRTEM), Buseck and Huang [6] found short, contorted layers in the carbon from shungites indicating a relatively low degree of crystallinity. On the basis of transmission electron microscopy, Kovalevski [29] proposed that carbon in shungites contains globular units that consist of curved layers that surround pores. Globular units were also described from type-I shungite by scanning tunneling microscopy [30].

It is evident that (a) the carbon in shungite rocks has attracted considerable interest over a long period of time, and (b) there are wide differences of opinion about its structural state and its relation to carbon from other geological environments and origins. The goal of this study is to compare the characteristics of the carbon in shungites to that of other poorly crystalline natural carbon. We used HRTEM, selected-area electron diffraction (SAED), and XRD to determine the structural features of the carbon in a range of shungite samples and to relate them to other natural sources of carbon. For some samples we used nanodiffraction, in which the electron beam of a scanning transmission electron microscope (STEM) is focused to a diameter of less than 1 nm to study the structure of small regions of thin samples.

2. Experimental

We studied a range of carbonaceous materials obtained from sedimentary and low-grade metamorphic rocks. The materials were labeled bitumen, pyrobitumen, asphaltum, impsonite, albertite, anthracite, anthraxolite (which, following Mancuso et al. [31], we hereafter will call pyrobitumen), natural coke, meta-anthracite, and shungites from different localities (Table 1). We measured carbon from shungite rocks from veins (Maksovo, Shunga, and

Chebolaksha), conformable lenses (Nigozero and Zazhogino), quartz geodes (Suisari), and drill holes (Maksovo), as well as carbon from types-I, -II, and -III shungite rocks from Shunga, Maksovo, and Chebolaksha. The various locations are given in Buseck et al. [11].

Carbon particles were separated from the raw samples by crushing and then hand picking. The isolated particles were finely ground and prepared as samples for XRD, TEM, and STEM study. XRD patterns were obtained with a Rigaku diffractometer using CuK_α radiation. The thin powder samples were placed onto an oriented mono-crystalline quartz plate and scanned from 10 to 90° 2θ, at a speed of 1 degree min^{-1}; signals were recorded at intervals of 0.02° 2θ. Apparent full width at half maximum (FWHM) values and peak positions were determined through deconvolution of the X-ray peaks with a combination of Gaussian and Lorentzian profiles as determined by using the software provided with the diffractometer. Apparent coherent lengths, L_c and L_a, were deduced from the FWHM values by using the Scherrer equation [$L = k\lambda/(B \cos\theta)$], where λ is the wavelength of the CuK_α radiation (0.154178 nm), θ is the Bragg angle, B is the FWHM value of the respective peaks, and k is a constant with values of 0.9 and 1.84 for the *002* and *110* peaks, respectively. The value of B was calculated by subtracting the instrumental from observed peak broadenings. The instrumental broadening of the *002* and *110* peaks (located at about 26° and 80° 2θ) was determined from an X-ray pattern of a thin powder sample of graphite as 0.16° and 0.25° 2θ, respectively.

A JEOL 4000 EX electron microscope was used for the HRTEM and SAED investigation. The powdered samples were placed onto lacy carbon films deposited on copper grids. Images and diffraction patterns were recorded photographically, digitized, and the digital HRTEM images were scanned perpendicular to the fringes and profiles were plotted. The images were calibrated with an HRTEM image of graphite using the same experimental conditions as for the unknowns, and individual spacings were determined from the calibrated distances between adjacent fringes.

SAED patterns were obtained for 400 kV electrons at a 2.5 nm*mm microscope constant (1.5 m specimen-to-plate distance). The FWHM of the first and third rings, close to the theoretical positions of the *002* and *110* rings of graphite, were determined according to the method of Rymer and Fayers [32]. The FWHM of the rings is influenced by instrumental effects, the finite particle, strain and distortion, and dynamic diffraction, as well variations of structural parameters from one particle to another. Instrumental effects and dynamic diffraction should be negligible for poorly crystalline carbon [32]. The finite particle or turbostratic stack size and strain effects can not be correctly interpreted for such samples by using FWHMs because only a few rings are available. We assign FWHMs to the stack-size effect and estimate apparent SAED

coherent lengths, L_c and L_a, only for comparisons with respective X-ray values.

A Vacuum Generators HB-5 STEM was used to study the carbon in selected samples of shungite by bright- and dark-field images. Some bright-field STEM images were made at high resolution (0.3 to 0.5 nm, depending on the amount of vibrational interference that existed at the time in the microscope), and then the same areas were examined at low resolution (0.7 to 1 nm) using the same small objective aperture used to take nanodiffraction patterns [33]. A series of nanodiffraction patterns was recorded on video tape as the beam was scanned slowly along a line in the image, usually about 74 nm long in 10 s, so that one diffraction pattern was recorded for each 0.3 nm movement of the beam, which was about 0.7 nm in diameter.

3. Results and discussion

3.1. Transmission electron microscopy

We grouped the poorly crystalline carbon samples based on their structural ordering as seen in their SAED patterns and HRTEM images. The SAED patterns are all of powders; some of their diffraction rings are circular whereas others are elliptical, indicating a strong preferred orientation about a common c-axis that is tilted with respect to the incident electron beam [34]. HRTEM images show fringes representing individual carbon layers (graphene layers) and resemble those of carbonaceous materials obtained from kerogens [17] and low-grade metamorphic rocks [6]. Rather than attempting to reproduce SAED patterns and HRTEM images from all samples we studied, the figures are of samples selected as representative of the various groups.

The grouping of the samples is somewhat arbitrary, and the characteristics of the groups tend to merge into one another. Moreover, bitumen, pyrobitumen, and albertite, among others, appear to consist of more than one microconstituent. We received and examined a variety of samples labeled pyrobitumen, and they exhibit a wide range of structural organization, suggesting that pyrobitumen is more aptly used as a geological than a structural term. Although we decided to retain the original terminology, we are not satisfied that it provides adequate precision. The HRTEM images in the figures are from the
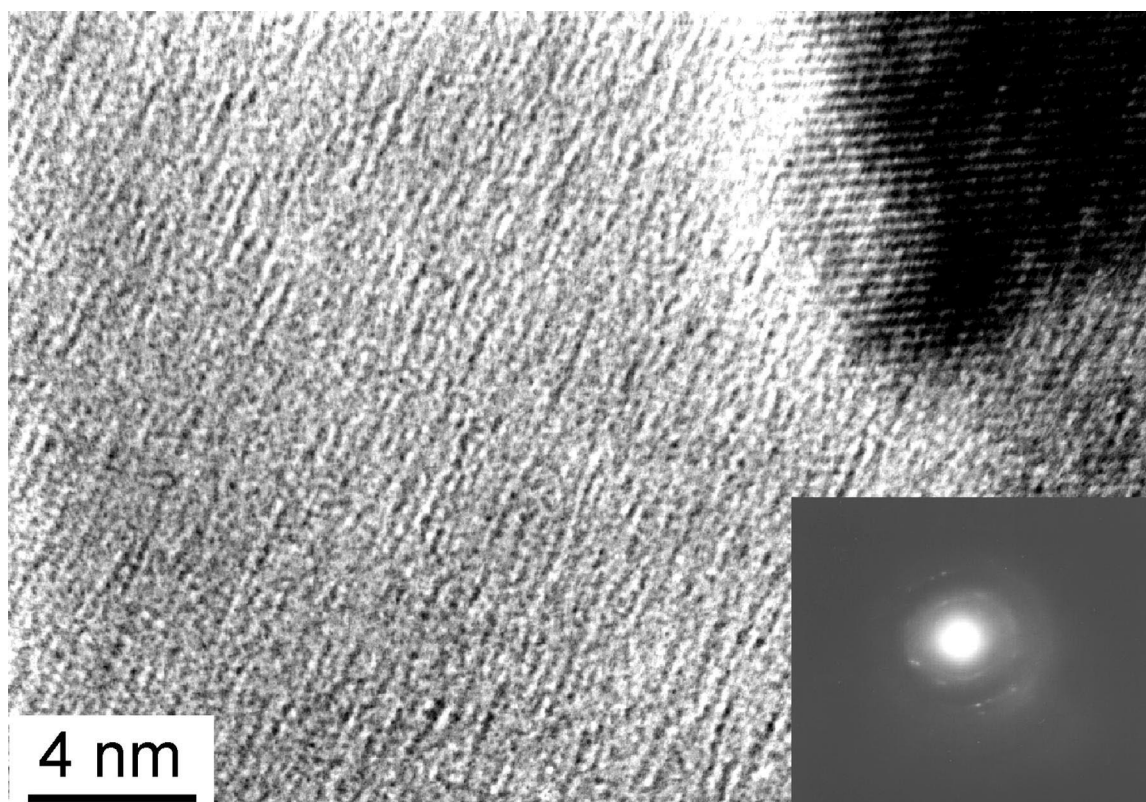

Fig. 1. HRTEM image of bitumen (Petroleum Springs). The fringes are short, slightly irregular but roughly parallel, and up to 3 nm in length. Long, straight, parallel fringes in the upper right are from an unidentified impurity crystal. The inserts in this and subsequent figures are SAED patterns.

samples with the greatest structural order for that sample type. Average structural parameters obtained from SAED patterns and HRTEM images are given in Table 1.

The first group is represented by bitumen. Its SAED patterns display weak intensities and diffuse maxima that indicate a low degree of order. Fig. 1 shows an HRTEM image of the bitumen. A striking feature is the short, slightly irregular but roughly parallel fringes from 1 to 3 nm in length. These fringes are similar to those caused by translation of the sample under the electron beam, but the fringes from the impurity crystal in the upper-right corner of Fig. 1 shows that shifting did not occur. The spacings between fringes (d_f) exhibit a considerable range, from 0.36 to 0.5 nm. The combination of relatively poor layer definition and their roughly parallel orientation in different packets suggests the bitumen may have been exposed to directed external pressure.

Group-2 samples consist of asphaltum, albertite, and pyrobitumens from the Hatyspyt Formation and Elliot Lake. The innermost *002* SAED maximum of these samples is poorly defined, and the *100* and *110* rings are diffuse. HRTEM images of the asphaltum and albertite are characterized by stacks of two to three layers, with lengths up to 1.5 nm. Random bending of fringes occurs. An

HRTEM image of the pyrobitumen resembles that of the bitumen, but the fringes are slightly longer (Fig. 2). In places there are incipient stacks of two to four fringes with lengths up to 2 nm. The distance between fringes is from 0.35 to 0.47 nm for the pyrobitumen from the Hatyspyt Formation and about 0.50 nm for pyrobitumen from Elliot Lake.

Group-3 samples contain asphaltite, impsonite, cannel coal, and pyrobitumen, all of which have circular rings in their SAED patterns. The *002* maxima are sharp but weak. The *100* and *110* maxima are poorly defined and diffuse. The HRTEM images of the impsonite contain layer fragments that form column-like stacks of 5 to 10 layers, with lengths of about 1 nm (Fig. 3). The HRTEM images and SAED patterns of the cannel coal resemble those of impsonite, but they contain thicker stacks (8 to 12 layers). Soot-like (onion-like) particles about 30 nm in diameter occur in the cannel coal.

We studied three pyrobitumen samples from the Gunflint formation, Ontario, Canada. They are from different collections (UCLA, Harvard, and Bowling Green Universities) but display similar macroscopic characteristics. HRTEM images of two of the samples show long twisted layers that form column-like stacks up to seven layers
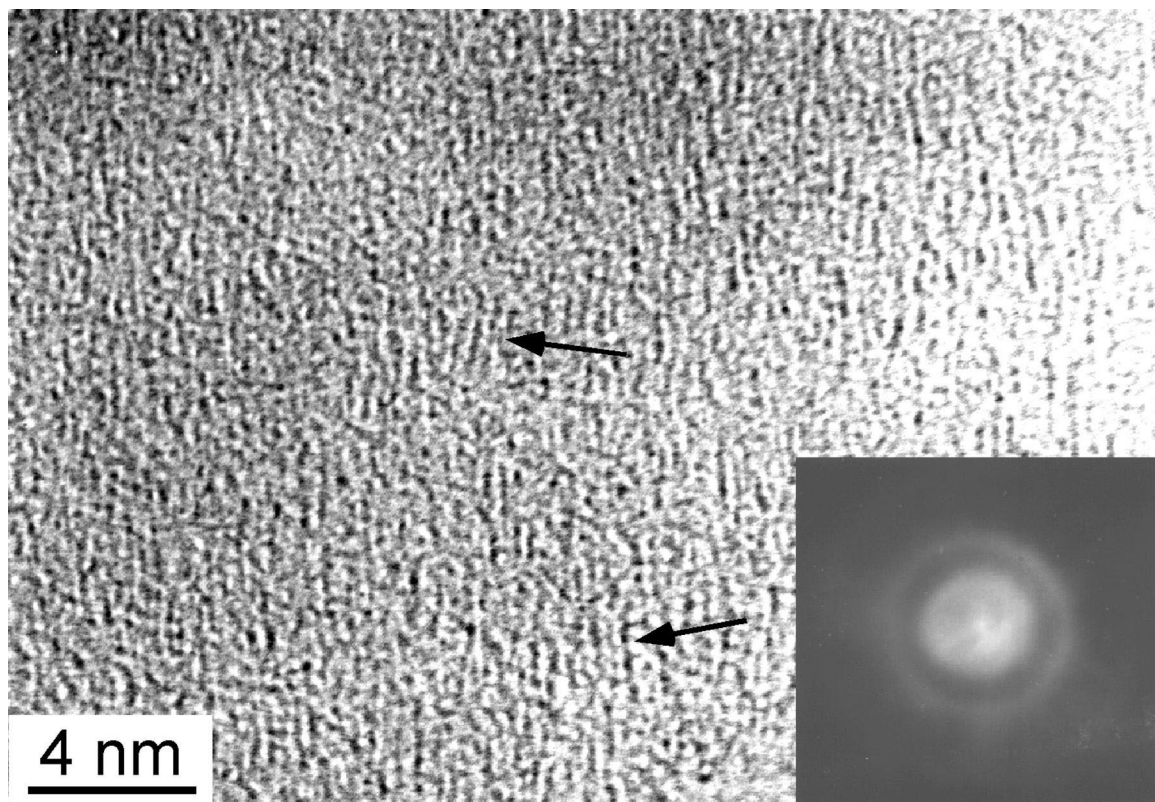

Fig. 2. Representative HRTEM image of group-2 samples (pyrobitumen, Hatyspyt formation). Poorly defined stacks (arrowed) with up to four layers and lengths up to 2 nm occur. The *002* SAED maximum is poorly defined; the *100* and *110* rings are well defined but diffuse.
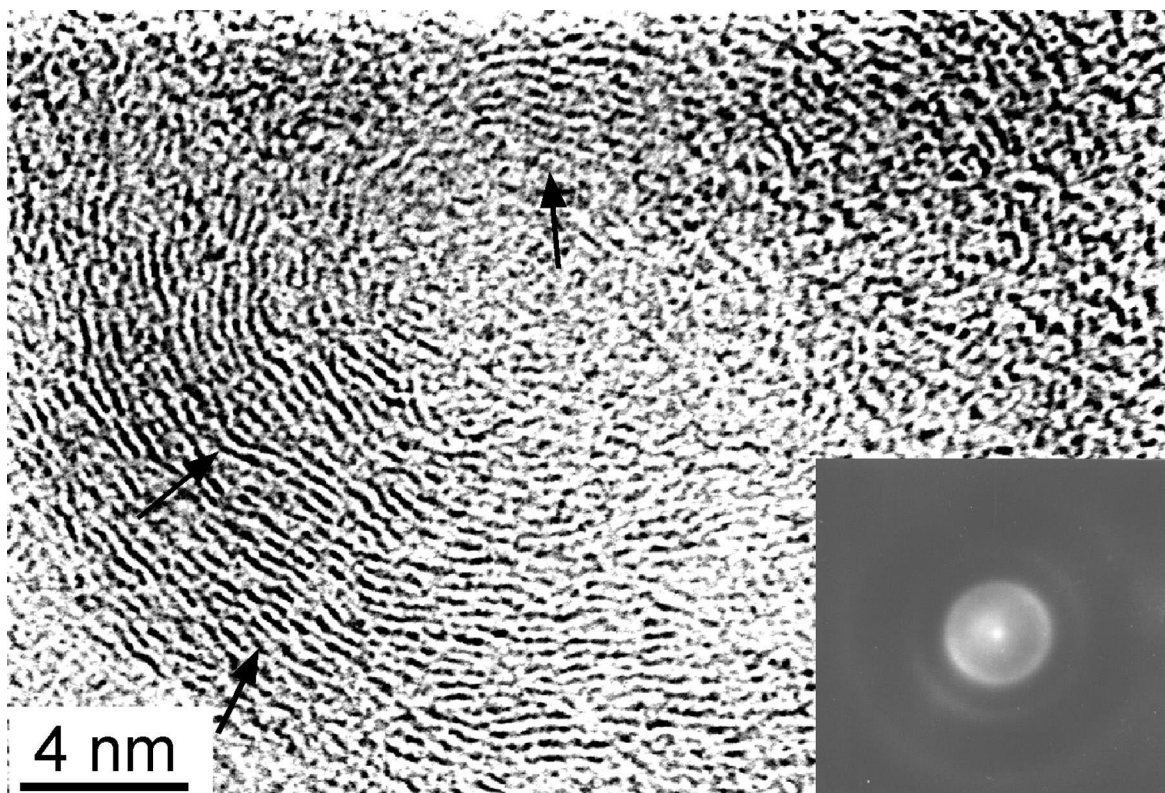
Fig. 3. Representative HRTEM image of group-3 samples (cannel coal, Wigan, UK). Layer fragments form column-like stacks (arrowed) of five to 10 layers with lengths of about 1 nm. The *002* SAED maximum has low relative intensity and is narrow. The *100* and *110* maxima are well defined but diffuse. All SAED maxima are circular.

thick, with lengths of about 1 nm. The third sample shows the same features, but with narrower stacks.

Group-4 contains adamsite, anthracite, meta-anthracite, pyrobitumen and carbonaceous matter from the Bakyrchik gold-bearing deposit. The rings in their SAED patterns are elliptical, with diffuse maxima. The HRTEM images show curved, interlaced layers in stacks formed by five to six layers, with lengths of about 2 nm (see arrows on Fig. 4); in places the stacks are connected to one another by layers up to 10 nm long. The five anthracites listed in Table 1 have individual layers from 10 to 20 nm long as well as stacks containing between three and eight layers 2 to 3 nm in length. The sample from the Primrose Seam is unusual in that its layers are curved and nested, much like the layers in onions. Carbonaceous matter from the Bakyrchik gold-bearing deposit had been classified on the basis of its SAED pattern as shungite [35], but the HRTEM images show that it is closer to anthracite than shungite (Table 2).

Group-5 samples contain natural coke, carbon from several gold mines, the Sudbury impact structure, and from the shungites. The *002* maxima of the SAED patterns of all group-5 samples are either asymmetric or else symmetric and broad. All other SAED maxima (*100* and *110*) are well defined and relatively narrow. All images contain

well-defined fringes (Fig. 5), and these occur in packets of 5 to 14 layers. Many of the layers are curved, and in places they appear as if they might close upon themselves to form pores, although the tangle of intervening layers makes such an interpretation uncertain. In previous work, Buseck and Huang [6] also found open spaces in the carbon from what they called chert associated with the shungite. Using terminology consistent with the Russian literature (Buseck et al. [11]), this sample was of the lydite variety of type-V shungite.

The carbon in shungite and that in synthetic coke (e.g., Fig. 11 from [10] of *p*-terphenyl coke heated to 2500°C) look almost identical in HRTEM images; we believe both are examples of what Franklin [36] called non-graphitizing carbons.

3.2. X-ray measurements

The diffraction peaks of all poorly crystalline carbons are, by definition, ill defined. However, the end product of geologic processing of such samples is graphite. Moreover, many of the intensity maxima of such carbons fall in the approximate positions of graphite peaks. Recognizing this crystallization trend and structural relation, we shall refer
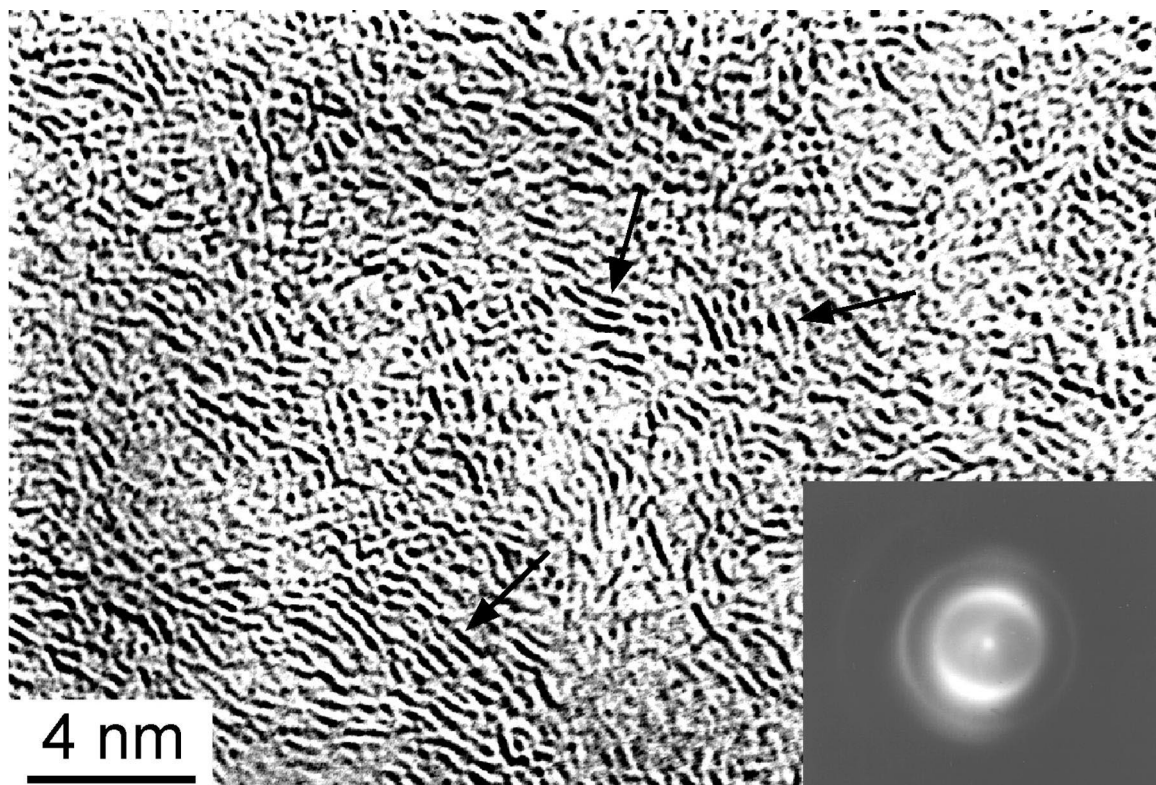
Fig. 4. Representative HRTEM image of group-4 samples (anthracite, Chrustaljnaja, Russia). Stacks of 2 to 10 curved, interlaced layer fragments occur. Their lengths range from 1.5 to greater than 3 nm. The *002*, *100*, and *110* SAED maxima are noticeably elliptical and rather diffuse.

to the several maxima of the poorly crystalline carbons with the indices of graphite although the lack of strict equivalence is apparent.

XRD patterns of the various groups are shown in Fig. 6. They are typical of turbostratic layering. The bitumen, asphaltum and pyrobitumen from Hatyspyt and Elliot Lake areas are exceptions in which only a broad feature is observed instead of the *002* peak (Fig. 6a), reflecting their poor structural organization. Adamsite, albertite, asphaltite, impsonite, and cannel coal are marked by doublet peaks close to the *002* position of graphite (Fig. 6b). The first peak is wide and shifted to low angles, similar to that of bitumen and pyrobitumen. The second peak is narrower and shifted slightly from the *002* graphite peak position. The other peaks are very broad.

The XRD patterns of natural coke and pyrobitumen samples from the Gunflint formation have relatively narrow first peaks, with minimal shifts from the *002* graphite position but wide *100* and *110* maxima (Fig. 6c). Anthracites and pyrobitumen from Mesabi are characterized by narrow *200* peaks shifted to lower angles and wide *100* and *110* peaks (Fig. 6d). Meta-anthracite, carbonaceous matter from the Bakyrchik and Sovetskaya gold deposits, pyrobitumen from the Sudbury impact structure, and

material sent to us as graphite (Erickson gold mine, Canada; [37]) but better described as poorly crystalline graphitic carbon, are unusual in having wide *002* peaks at 0.345 to 0.351 nm and FWHM equal to 4.2–6.2° 2θ Cu. The *100* and *110* peaks are not as wide as those of natural coke, pyrobitumen, and anthracites (Fig. 6e).

The carbons from all shungite samples we studied have similar X-ray parameters, independent of their source localities and shungite types. Their XRD patterns are characterized by broad peaks with spacings from 0.346 to 0.352 nm, close to that of graphite *002*; their FWHM values range from 4.2 to 6.4° 2θ Cu (Fig. 6e). The XRD peaks close to the *110* graphite peak have spacings of about 0.122 nm and FWHM from 3.9 to 6.0° 2θ Cu.

Samples such as coke show an apparent discrepancy in that the relative intensities and widths of the corresponding rings and peaks are reversed between the SAED and XRD patterns. These results reflect differences in the sizes of the regions giving rise to the diffraction patterns (about 1 mm for X-rays and 1 μm for SAED) relative to the sizes of the coherently diffracting stacks. Discrepancies between the two types of patterns may be expected if these correlation ranges lie between 1 micrometer and 1 millimeter. The observation of elliptical rings in some SAED patterns, for

Table 2
Sources of the samples listed in Table 1

Sample type	Locality	Sample no.	Source
Group 1			
Bitumen	Los Angeles, CA	24 375.0000	NMNH[a]
Group 2			
Asphaltum	Santa Barbara Co., CA	56 421.0000	NMNH
Albertite	New Brunswick, Canada	12 757.0000	NMNH
Pyrobitumen	Hatyspyt fm., Siberia		A. Knoll, Harvard
Pyrobitumen	Elliot Lake, Ontario		J. Mancuso, Bowling Green State U.
Group 3			
Asphaltite	Standard mine, CA	73 989.0000	NMNH
Impsonite	Maine		Ed Grew, U. Maine
Cannel coal	Wigan, UK	10 530.0000	NMNH
Pyrobitumen[b]	Gunflint fm., Canada	1377	W. Schopf, UCLA
Pyrobitumen	Gunflint fm., Ontario		J. Mancuso, Bowling Green State U.
Pyrobitumen[b]	Gunflint fm., Ontario		A. Knoll, Harvard
Group 4			
Adamsite	Atoka, Oklahoma	73 780	NMNH
Anthracite	Iserl, La Motte, France	46 403.0000	NMNH
Anthracite	Canada	33 311.0000	NMNH
Anthracite	Aveiro, Portugal	40 073.0000	NMNH
Anthracite	Primrose Seam, PA	PSOC-870	Penn State Coal Collection
Anthracite	Chrustaljnaja, Woodjanaja Ravine, Russia	59 342	NMNH
Pyrobitumen	Mesabi, Minnesota		J. Mancuso, Bowling Green State U.
Meta-anthracite	Michigamme shale, Michigan		A. Knoll, Harvard
Carbonaceous matter	Bakyrchik gold deposit, Kazakhstan		KRC, RAS[d]
Group 5			
Carbon from type-I shungite rock	Chebolaksha		KRC, RAS
Carbon from type-III shungite rock	Chebolaksha		KRC, RAS
Carbon from type-I shungite rock	Maksovo	SH95-M1a	ASU
Carbon from type-I shungite rock #1[e]	Maksovo		KRC, RAS
Carbon from type-I shungite rock #2[e]	Maksovo		KRC, RAS
Carbon from type-I shungite rock #3[e]	Maksovo		KRC, RAS
Carbon from type-I shungite rock #4[e]	Maksovo		KRC, RAS
Carbon from type-I shungite rock	Nigozero		KRC, RAS
Carbon from type-I shungite rock	Shunga		KRC, RAS
Carbon from type-II shungite rock	Shunga	SH95-S2c	ASU
Carbon from type-I shungite rock	Sujsari		KRC, RAS
Carbon from type-I shungite rock	Zazhogino		KRC, RAS
Carbon from type-III shungite rock	Zazhogino		KRC, RAS
Natural coke	Jewett Brothers Mine, Chesterfield Co., VA	63 499.0000	NMNH
Carbonaceous matter[c]	Erickson gold mine, Canada		Geol. Surv. Canada
Carbonaceous matter	Sovetskaya gold mine, Yenisej, Siberia		M.E. Generalov, Fersman Mineral. Museum, Moscow
Pyrobitumen[b]	Sudbury, Ontario	SURG2	D. Heymann, Rice U.
Pyrobitumen	Sudbury, Ontario		D. Heymann, Rice U.

[a] NMNH – U.S. National Museum of Natural History (Smithsonian Institution of Washington).

[b] These samples were received as anthraxolite.

[c] This sample was received as «graphite».

[d] Karelian Research Center of the Russian Academy of Sciences, Petrozavodsk, Russia.

[e] Shungites #1, #2, #3, and #4 are from veins cut by drill holes at Maksovo (Buseck et al., 1997, Fig. 2, 7). #1 – from layer C; #2 – from the interlayered tuffs; #3 – from the metadiabase; #4 – from the carbon-rich layer #1 (see Buseck et al., 1997, Figs. 2 and 7 for the locations of the layers and drill holes).
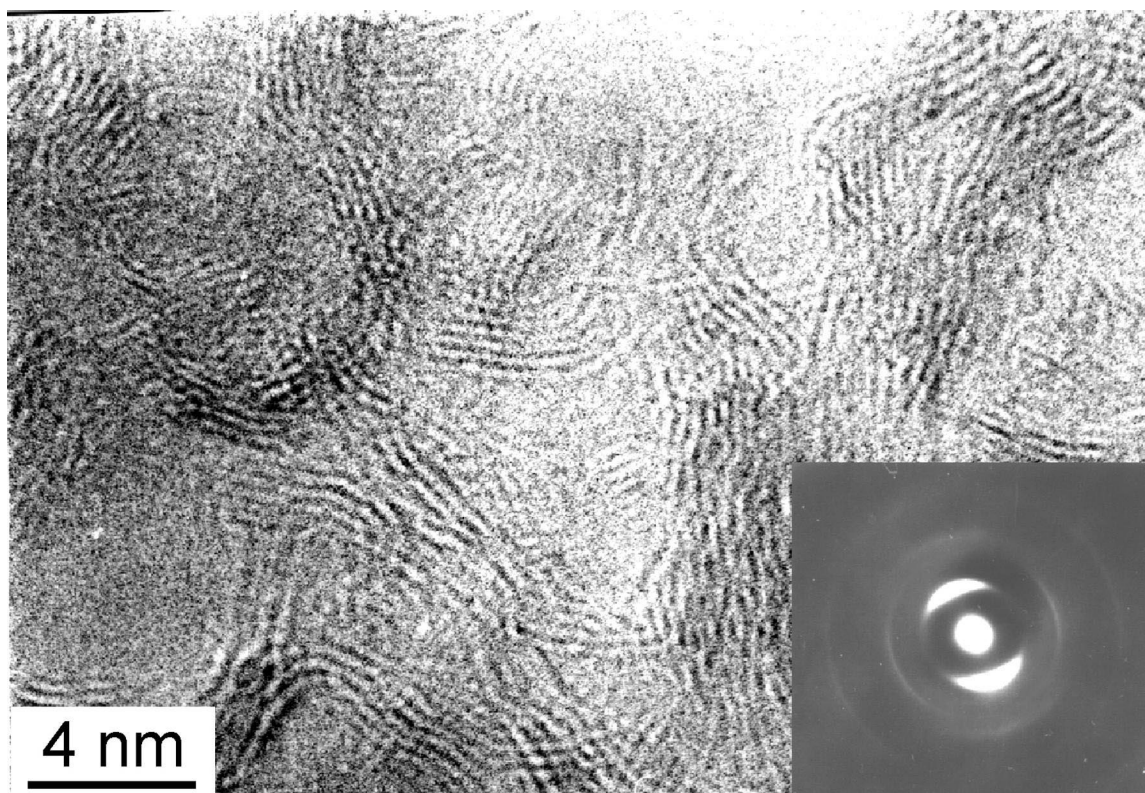
Fig. 5. Representative HRTEM image of group-5 samples (carbon from type-I shungite rock, Zazhogino). Bifurcating curved fringes occur in packets of 5 to 14 layers. SAED maxima occur at spacings close to graphite *00l* and *hk0*. The rings are broad and elliptical.

example, suggests that in those samples there is a strongly preferred orientation of the turbostratically stacked graphene layers relative to regions having dimensions of several micrometers for the thin samples used for electron microscopy. However, averaging over much larger regions obscures this feature with XRD measurements. It has been found by HRTEM that many noncrystalline specimens possess medium-scale structures that can contain voids, networks of pores, or variations in composition on the scale of 3 nm or more [38]. Bustin et al. [39] point out that graphitizing carbons have large domains (much wider than 1 micrometer), likely resulting from heterogeneity of the original sample composition. In contrast, carbon samples with small domains (less than 5 nm) are non-graphitizable [39]. Consequently, it appears as if the carbon in the shungite samples we studied is of the non-graphitizable variety [36].

The average number of stacked graphene layers and the uniformity of their spacings affect the widths of the *00l* reflections. The *hk0* reflections are influenced by the lateral extent and curvature of the graphene layers and also by the presence of both translational and rotational disorder (turbostratic structure) in the stacks, which tends to broaden the diffraction rings asymmetrically with extension towards the high-angle side.

Most samples we studied appear to have turbostratic stacking disorder of the graphene layers, as indicated by the HRTEM images that show extended arrays of parallel fringes with a 0.34 nm spacing and SAED patterns that show asymmetrically broadened and commonly elliptical *hk0* rings. For anthracite, the *00l* and *hk0* reflections and corresponding stack sizes are consistent between SAED and XRD patterns. For group-5 samples, other than coke, the *00l* reflections and corresponding L_c values are consistent between SAED and XRD patterns, but the *hk0* reflections and corresponding L_a values are slightly discrepant. Among the samples we studied, there is a tendency for the discrepancy to be less for anthracites and greater for coke. The differences among anthracite, coke and shungite must therefore be of a nature that is not readily determined from HRTEM and SAED observations and could arise, for example, from differences in the lateral extent or the frequency of bending of the stacks of graphene layers or from the nature of their stacking disorder.

3.3. Scanning transmission electron microscopy and nanodiffraction

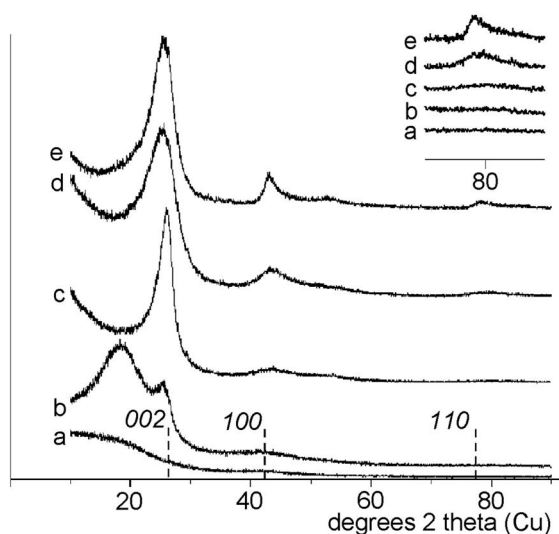Two shungite samples (from Nigozero and Zazhogino)

Fig. 6. Representative X-ray diffractograms of samples from each of the five groups: (a) Group-1: Pyrobitumen, Elliot Lake, Ontario; (b) group-2: Albertite, New Brunswick, Canada; (c) group-3: Pyrobitumen, Gunflint fm., Ontario (from J.Mancuso); (d) group-4: Anthracite, Chrustaljnaja, Russia; (e) group-5: Carbon from type-I shungite rock, Zazhogino. The insert shows *110* peaks of the samples. We defined the groups on the basis of their TEM characteristics, and in some cases there are seeming inconsistencies between their X-ray and SAED patterns. *002*, *100*, and *110* are positions of corresponding graphite peaks.

were studied using nanodiffraction and produced similar images. Many nanodiffraction patterns obtained with a stationary beam 0.7 nm in diameter show a line of spots through the origin corresponding to the 0.34 nm spacing of the stacking of the graphene layers, indicating that the illuminated region contains sets of layers almost parallel to the incident beam. In a few regions there are indications of *hkl* reflections, which correspond to 3-dimensional order in the stacking of the layers (as in graphite). Where present, these *hkl* reflections are weak, diffuse, and streaked parallel to the *00l* line, suggestive of disordered stacking. There are also rings that result from graphene layers that are approximately perpendicular to the incident beam. The rings corresponding to the *100* and *110* graphitic spacings are circular for layers perpendicular to the electron beam and become increasingly elliptical as the layers are tilted. The minor axes of the two ellipses reflect the *100* and *110* graphitic spacings. The ellipses become weaker and more diffuse, particularly in the direction of the major axes, as the stacking of the layers becomes less well ordered or if the layers are more strongly bent.

The STEM micrographs of group-5 samples (Fig. 7) suggest that they consist predominantly of highly disordered graphitic carbon. There is little evidence of amorphous carbon. The samples mainly consist of highly bent, disordered stacks of three to seven layers.

Information regarding the form of the disorder may be

deduced from micrographs on the assumption that the ordering in the beam direction is similar to that in the plane of the image. If that assumption is valid, then where the electron micrographs approximate closed loops of 0.34 nm fringes, we infer that the 3-dimensional structures may approach closed, 3-dimensional shells that are, in general, irregular rather than near-circular in cross-section. Similar closed loops of fringes have been observed and interpreted in this way in the case of the nanoparticles, or «nanoshells», formed in conjunction with carbon nanotubes in samples prepared by carbon arc evaporation (e.g. Ando and Iijima [40]; Cowley and Kiang [41]). There are more regions where the fringes do not form complete loops in the micrographs, and here the stacked graphene layers only form fragments of shells, connected to more-or-less flat regions. In many places the bends in the stacks are relatively sharp, with flat regions between the bends. Bends of 60 to 150 degrees occur over distances of 2–5 nm. Regions uniformly bent over distances of 10 nm or more are rare.

The observations from nanodiffraction patterns are consistent with deductions from the micrographs (Fig. 7). Sets of nanodiffraction patterns were recorded as the beam was scanned along selected lines in the STEM images for two regions that were thin extensions from the edges of thicker clumps of material. These were selected as typical of regions having high and intermediate degrees of ordering into approximate shells.

The results of the observations are summarized in Fig. 8a and b (plots 1 and 2). The intensities of the *00l* lines of spots are roughly indicated by the solid line for positions about 3 nm apart (every tenth frame of the video tape). The values of the ellipticity (axial ratios) are indicated by the dashed line. The thin horizontal line represents the average ellipticity imposed on circular rings by distortion in the imaging of the patterns by the post-specimen lenses in the microscope. Positive and negative deviations from this average represent tilts of the layers parallel or at right-angles to the direction of the average major axes. The strengths and directions of the *00l* lines of spots correspond to sets of 0.34 nm fringes in the images. The ellipticity of the rings suggests tilts of the layers, which is consistent with 3-dimensional configurations of the layers that might have been deduced from the STEM images. For example, at the extreme left of both plots in Fig. 8 the ellipticities of the *100* and *110* rings, and hence the tilts of the layers, are seen to be high just to the right of the regions at the outer edges of the shell images, where *00l* spots are strong and the beam is parallel to the layers. This interpretation is consistent with the proposal that the layers are bent into 3-dimensional shapes approximating closed or partly closed shells of rather irregular cross section.

Fig. 7 suggests a group of near-spherical shells with little overlapping material. There are also micrographs that suggest a much less perfect shell structure. Correspondingly, the nanodiffraction patterns taken along the scan lines show strong *00l* reflections where the micrographs show
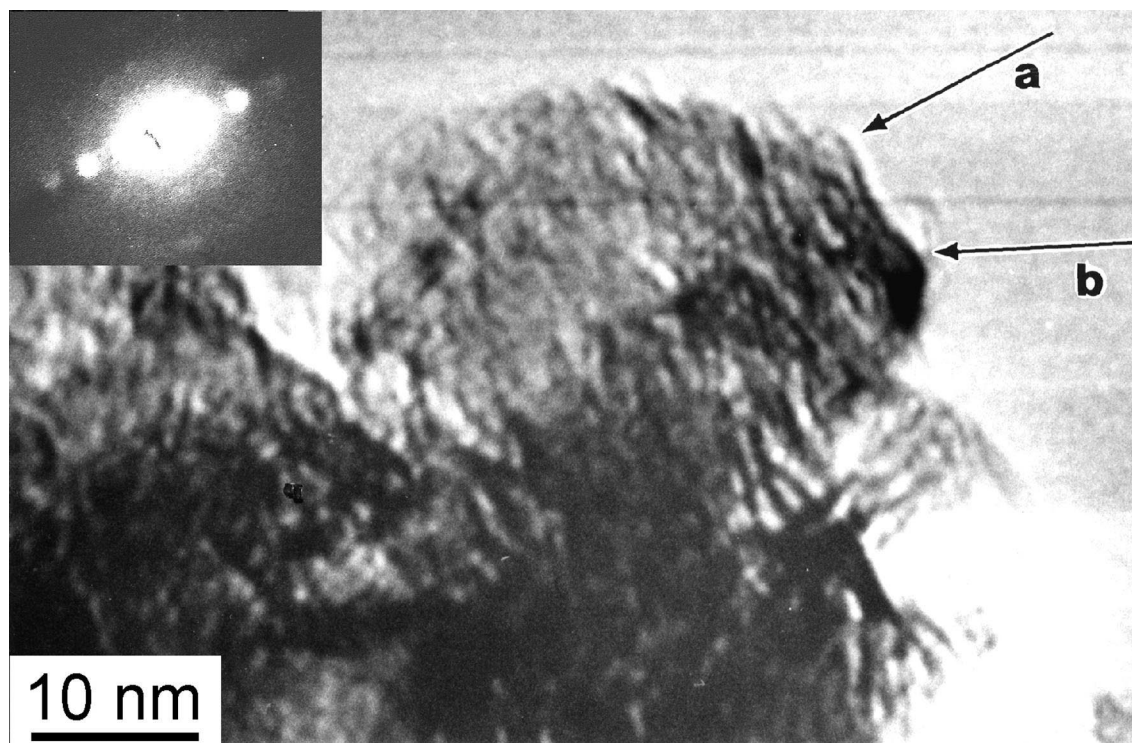
Fig. 7. STEM image of a thin region at the edge of carbon from a piece of shungite from Zazhogino. The arrows indicate the scan lines along which nanodiffraction patterns were recorded. The insert shows a nanodiffraction pattern from a region 0.7 nm in diameter that shows weak elliptical rings and the *00l* spots corresponding to the 0.34 nm layer-stacking distance.

sets of parallel fringes, and the ellipticities of the *100* and *110* rings suggests that the layers are tilted near those regions. But in many cases there are only weak, diffuse *00l* spots, as if the layers have highly disordered stacking and almost random orientations, as also suggested by the micrographs.

Thus, the nanodiffraction patterns are consistent with deductions made from looking at the STEM and HRTEM micrographs. A small proportion of the shungite samples have the form of sets of parallel stacks of graphene layers wrapped into rather irregular closed shells. More commonly, the sets of graphene layers form only fragments of such shells or are heavily bent into irregular non-closed shapes. For much of the sample, there is little regular stacking of the layers. Individual layers are crumpled and not aligned.

4. Conclusions

Although there is a wide range of types of shungite rocks, and shungites occur in widely separated regions in Karelia, it appears as if the structure of their carbon is similar throughout with respect to both HRTEM images and SAED patterns. Other samples whose carbon is indistinguishable using these techniques include those from

the Erickson gold mine (Canada), the Sovetskaya gold mine (Russia), and the Sudbury impact structure (Ontario). Carbon from different localities of the Shunga district is characterized by its curved layers, similar to samples of natural and synthetic cokes. They possesses turbostratic stacking of the graphene layers. The carbon from the shungite samples appears to be structurally homogeneous on a scale between 1 μm and 1 mm and, adopting the terminology of Franklin [36], they seem to be of the non-graphitizable variety of carbon.

The HRTEM images of shungites suggest that some 3-dimensional closed shells occur but, more commonly, there are fractions of such shells or regions of graphene structure that are highly disordered into short bent stacks. The 3-dimensional structures that might be surmised from the HRTEM images are supported by the sets of nanodiffraction patterns.

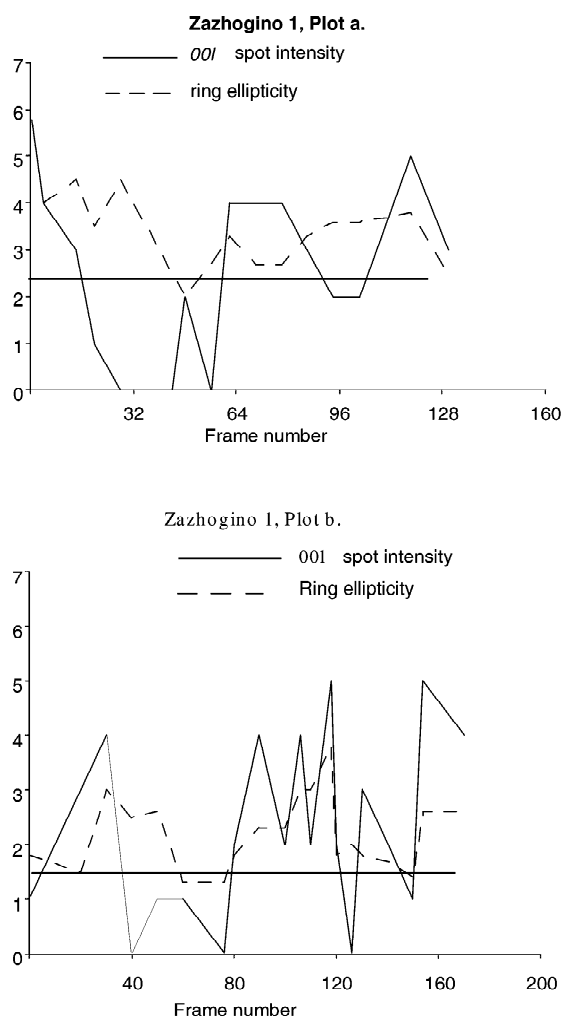**Zazhogino 1, Plot a.**

Zazhogino 1, Plot b.

Fig. 8. Plots of the intensities of the *001* spots and the ellipticities of the *100* and *110* rings of the nanodiffraction patterns, which were recorded along lines (a) and (b) indicated in Fig. 7 (ellipticity $= 10 \times [(b\text{-axis}/a\text{-axis}) - 1]$). The frame numbers, when multiplied by 0.3, equal distance in nanometers along the traverses.

References

[1] Landis CA. Graphitization of dispersed carbonaceous material in metamorphic rocks. Contrib Mineral Petrol 1971;30:34–45.

[2] Pacault A. In: Walker Jr. PL, editor, Chemistry and physics of carbon, vol. 7, New York: Marcel Dekker, 1971, pp. 107–54.

[3] Grew ES. Carbonaceous material in some metamorphic rocks of New England and other areas. J Geol 1974;82:50–73.

[4] Itaya T. Carbonaceous material in pelitic schists of the Sanbagawa metamorphic belt in central Shikoku, Japan. Lithos 1981;14:215–24.

[5] Bonijoly M, Oberlin M, Oberlin A. A possible mechanism for natural graphite formation. Int J Coal Geol 1982;1:283–312.

[6] Buseck PR, Huang B-J. Conversion of carbonaceous material to graphite during metamorphism. Geochimica et Cosmochimica Acta 1985;49:2003–16.

[7] Pasteris JD, Wopenka B. Raman spectra of graphite as indicators of degree of metamorphism. Can Mineralog 1991;29:1–9.

[8] Wopenka B, Pasteris JD. Structural characterization of kerogens to granulite-facies graphite: Applicability of Raman microprobe spectroscopy. Am Mineralog 1993;78:533–57.

[9] Wada H, Tomita T, Matsuura K, Iuchi K, Ito M, Morikiyo T. Graphitization of carbonaceous matter during metamorphism with references to carbonate and pelitic rocks of contact and regional metamorphisms, Japan. Contrib Mineral Petrol 1994;118:217–28.

[10] Buseck PR, Huang B-J, Keller LP. Electron microscope investigation of the structures of annealed carbons. Energy & Fuels 1987;1:105–10.

[11] Buseck PR, Galdobina LP, Kovalevski VV, Rozhkova NN, Valley JW, Zaidenberg AZ. Shungites: the C-rich rocks of Karelia, Russia. Can Mineralog 1997;35:1363–78.

[12] Buseck PR, Tsipursky SJ, Hettich R. Fullerenes from the geological environment. Science 1992;257:215–7.

[13] Inostrantsev AA. New extreme example in the series of amorphous carbon. Gornii J 1879;2:314–42 (in Russian).

[14] Timofeyev VM. About genesis of Shungite from the Onega region. Proc Leningrad Soc Natural 1924;39:40–50 (in Russian).

[15] Rankama K. New evidence of the origin of Pre-cambrian carbon. Bull Geologic Soc Am 1948;59:389–416.

[16] Volkova IB, Bogdanova MV. Petrology and genesis of Karelian shungite-high rank coal. Int J Coal Geol 1986;6:369–79.

[17] Buseck PR, Huang B-J, Miner B. Structural order and disorder in Precambrian kerogens. Org Geochem 1988;12:221–34.

[18] Cornelius CD. In: Meyer RF, editor, Exploration for heavy crude oil and natural bitumen, AAPG studies in geology, vol. 25, Tulsa, OK: Amer. Assoc. Petroleum Geologists, 1987, pp. 165–74.

[19] Meyerhoff AA, Meyer RF. In: Meyer RF, editor, Exploration for heavy crude oil and natural bitumen, AAPG studies in geology, vol. 25, Tulsa, OK: Amer. Assoc. Petroleum Geologists, 1987, pp. 31–99.

[20] Meyer RF, De Witt W. Definition and world resources of natural bitumens. US Geological Survey Bulletin 1944, 1990.

[21] Jehlicka J, Rouzaud JN. In: Parnell J, Kucha H, Landais P, editors, Bitumens in ore deposits, Berlin: Springer Verlag, 1993, pp. 53–60.

[22] Parnell J, Carey PF, Bottrell SH. The occurrence of authigenic minerals in solid bitumens. J Sedim Res 1994;A64:95–100.

[23] Moroz LV, Arnold G, Korochantsev AV, Wasch R. Natural solid bitumens as possible analogs for cometary and asteroid organics. Icarus 1998;134:253–68.

[24] Khavari-Khorasani G, Murchison DG. The nature of Karelian shungite. Chem Geol 1979;26:165–82.

[25] Melezhik VA, Fallick AE, Filippov MM, Larsen O. Karelian shungite-an indication of 2000 Ma-year-old metamorphosed oil-shale and generation of petroleum: geology, lithology and geochemistry. Earth-Sci Rev 1999;47:1–40.

[26] Boldyrev AK, Kovalev GA. X-ray study of shungite, anthracite, and coal. Zapiski LTI 1937;10:3–51 (in Russian).

[27] Kviecinska B. Investigations of shungite. Bull Pol Acad Sci (Chem) 1968;16:61–5.

[28] Usenbayev K, Zhumaliyeva K, Ruskulbekova R, Kalinin Yu. Structure of the 1st type shungite. Doklady Akademii Nauk USSR 1977;232:1189–92 (in Russian).

[29] Kovalevski VV. Structure of shungite carbon. Russ J Inorg Chem 1994;39:28–32.

[30] Yushkin NP. Globular shungite structure: Tunnel electron microscopic data. Doklady Russian Academii Nauk 1994;337:800–3 (in Russian).

[31] Mancuso JJ, Kneller WA, Quick JC. Precambrian vein pyrobitumen: evidence for petroleum generation and migration 2 Ga ago. Precambr Res 1989;44:137–46.

[32] Rymer TB, Fayers FJ. The intensity profiles of electron diffraction lines. Phil Mag 1958;3:1137–53.

[33] Cowley JM. Electron nanodiffraction. Micros Res Techniq 1999;46:75–97.

[34] Schiffmaker G, Dexpert H, Caro P, Cowley JM. Elliptic electron diffraction patterns from thin films of «turbostratic» graphite. J de Microscopie et de Spectroscopie Electroniques 1980;5:729–34.

[35] Marchenko LG, Kovalevski VV. Carbonaceous matter in the gold-bearing deposit. Doklady Akademii Nauk USSR 1984;279:982–5 (in Russian).

[36] Franklin RE. Crystallite growth in graphitizing and non-graphitizing carbons. Proc Roy Soc Lond 1951;A209:196–218.

[37] Mastalerz M, Bustin RM, Sinclair AJ, Stankiewicz BA. Carbon-rich material in the Erickson hydrothermal system, Northern British Columbia, Canada: Origin and formation mechanisms. Econ Geol 1995;90:938–47.

[38] Howie A. In: Buseck PR, Cowley JM, Eyring L, editors, High-resolution transmission electron microscopy, New York, Oxford: Oxford University Press, 1988, pp. 607–32.

[39] Bustin RM, Rouzaud J-N, Ross JV. Natural graphitization of anthracite: experimental considerations. Carbon 1995;33:679–91.

[40] Ando Y, Iijima S. Preparation of carbon nanotubes by arc-discharge evaporation. Jap J Appl Phys 1993;32:L107–109.

[41] Cowley JM, Kiang C-H. The structure of near-spherical carbon nanoshells. Carbon 2000 (in press).